506 KSME Journal, Vol. 9, No. 4, pp. 506~514, 1995

Streaming Flow Induced by Two Oscillating Circular Cylinders

Yong Kweon Suh*

(Received May 2, 1995)

Two-dimensional Stokes flow generated by an acoustic streaming around two circular cylinders were studied. A series solution method is developed to obtain both the potential and Stokes flows. Calculation results for two equal cylinders show that the streaming flow pattern undergoes six bifurcations with the direction of the oscillatory motion of the fluid when two bodies are at moderate or large distance. When they come closer, the pattern becomes more complicated especially in the gap region. The present solution method can be easily extended to an arbitrary arrangement of multiple circular cylinders with different radii.

Key Words: Streaming Flow, Two Circular Cylinders, Stokes Flow, Series Solution

1. Introduction

It is well known that, when a solid body performs small-amplitude, high-frequency oscillation in a viscous fluid that is otherwise at rest, the fluctuating motion of the body is felt only in the thin 'Stokes' layer developed near the body surface, and the outside region is governed by a steady streaming flow induced by the nonlinear effect in the layer. Although the streaming flow is weaker than the the flucuating one, it plays a dominant role in migration of particles (Batchelor, 1967) and heat/mass transfer (Krasuk and Smith1963, Davidson 1973, Haddon and Riley 1981). Fortunately, the velocity at the edge of the layer that drives the outside flow can be obtained without actually solving the Stokes-layer equations. We only need to solve the potential-flow problem constituted by a uniform flow past the body along the direction of oscillation. It is this feature that intrigues the fluid dynamicist. A nice introduction and survey of the early literature has been given by Riley (1967).

The historically diversified works on the subject may be categorized by the three factors; first, the number of bodies and their arrangement, second, the shape of the body, and third, the order of the streaming Reynolds number, R_s (R_s is based on the streaming velocity at the body surface). The earliest, fundamental model, that gives the simplest closed form solution, is a circular cylinder in the limit of low R_s. This model, then, has been extended to the moderate and large R_s. It is now well known that increase of R_s in the model can even change the flow direction in the far field (Stuart, 1966). Recently, there have been some investigations for bodies which take other shapes. Pattani and Olson (1987) obtained numerical solutions for the square and Joukowskii profiles at $R_s<4$. Kim and Troesch (1989) also obtained numerical solutions for the square and asymmetrical bodies at $R_s<100$. Their results imply that the noncircular shape can generate complex flow patterns. The flow pattern can also be diversified by the number of bodies and their arrangement. Two-circular-cylinder problem in the low R_s limit has been solved by Zapryanov, Kozhoukharova and Iordanova (1988) for two special cases. It was shown that depending on the cylinder size difference and the distance, the flow pattern can change significantly. A cascade of circular cylinders at $R_s<100$ has been investigated by Yan, Ingham and Morton (1993). It was observed that a breakdown of symmetry in the streaming flow occurs at the critical value of R_s between 8 and 9.

In this work, streaming flow around two cir-

* Department of Mechanical Engineering, Dong-A University Pusan 604-714, Korea

cular cylinders in the low R_s limit is investigated. As mentioned above, Zapryanov, Kozhoukharova and Iordanova (1988) have studied the same problem, but their solution methods are applicable only to two special cases; one, two different cylinders oscillating parallel to the plane containing their axes, and two, the equal cylinders oscillating perpendicular to the plane containing their axes. In this work, methods are developed to consider the most general cases in which both the cylinder size difference and the direction of oscillation are varied without any restriction.

The stream function for both the potential and Stokes flow is represented basically by the sum of two functions, each of which uses the separate coordinate system. Method of successive improvement is used to obtain the converged solutions.

2. Formulation of the Problem

As usual, we fix the coordinates on the bodies and regard the fluid as oscillating with velocity $U_0 \sin\omega t$ at infinity. The traditional nondimensional numbers, which characterize the governing equations and the corresponding flow are;

$$\varepsilon=\frac{U_0}{\omega a},\ M^2=\frac{\omega a^2}{\nu},\ R_s=\frac{U_0^2}{\omega\nu}, \tag{1}$$

where a is the radius of the larger cylinder and ν the kinematic viscosity of the fluid. These can be derived by taking a, $1/\omega$ and U_0 as the length, time and velocity scales. ε represents the amplitude of oscillation relative to a and M^2 the diffusion time scale $O(a^2/\nu)$ relative to the time scale of oscillation $O(1/\omega)$. As stated in §1, we assume $\varepsilon\ll 1$, $M^2\gg 1$, and $R_s\ll 1$.

Applying the asymptotic perturbation techniques then gives the nondimensional governing equations for the $O(\varepsilon)$ streaming flow as follows.

$$\nabla^4\Psi=0, \tag{2}$$

where Ψ is the $O(\varepsilon)$ nondimensional stream function and ∇^4 is the biharmonic operator. Hereinafter all the quantities are dimensionless otherwise specified. As shown in Fig. 1, the Cartesian coordinate system (x,y) has its origin at the center of the upper cylinder.

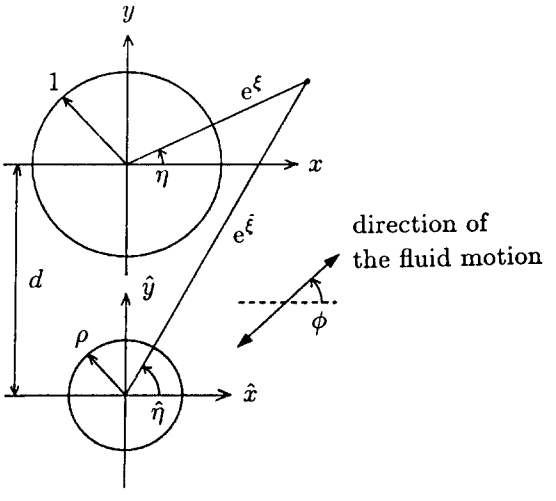

Fig. 1 Configuration of arrangement of two circular cylinders subject to a two-dimensional periodic flow, and two separate coordinate systems.

The boundary conditions at the body surface can be written as

$$\frac{\partial\Psi}{\partial s}=0, \tag{3a}$$

$$\frac{\partial\Psi}{\partial n}=u_s=-\frac{3}{4}u_p\frac{du_p}{ds}, \tag{3b}$$

where s and n are coordinates along and normal to the body surface, and u_p and u_s are the potential and streaming velocities at the body surface (e.g. Riley, 1967). The boundary conditions at infinity are rather subtle by the following reasons. For the two-dimensional, unbounded flow, two paradoxes are known. The Stokes paradox states that there is no solution to the biharmonic equation that satisfies both the noslip condition on an isolated-body surface and a uniform flow at infinity. The Jeffery paradox (Jeffery, 1922) states that the locally generated flow around isolated bodies can generate a uniform flow at infinity. These simply imply that specifying arbitray boundary conditions at infinity may lead to an ill-posed boundary-value problem. In view of this, we simply require the slowest possible flow at infinity (Smith, 1990).

Three parameters that determine the flow characteristics are; ϕ, angle of the direction of oscillation, d, distance between two cylinders, and ρ,

radius of the lower cylinder ($\rho \leq 1$).

3. Potential Flow Solution and the Surface Streaming Velocity

We first need to solve the potential flow problem constituted by a uniform flow past the two cylinders along the same direction as the oscillatory motion of the fluid. We may use the bipolar coordinate system in view of the body arrangement. However, as we shall discuss in §4, this coordinate system is not suitable for the Stokes flow solution. So, to be consistent with the later development, we use two separate coordinate systems (x,y) and $(\hat{x},\hat{y})$ each of which has its origin at the center of each cylinder. These coordinates are then transformed to (ξ,η) and $(\hat{\xi},\hat{\eta})$ as follows.

$$z=e^{w},\quad \hat{z}=e^{\hat{w}}, \tag{4}$$

where $z=x+iy$, $\hat{z}=\hat{x}+i\hat{y}$, $w=\xi+i\eta$ and $\hat{w}=\hat{\xi}+i\hat{\eta}$ are complex coordinates and the relation $z=\hat{z}-id$, or

$$e^{\xi}\cos\eta=e^{\hat{\xi}}\cos\hat{\eta}, \tag{5a}$$

$$e^{\xi}\sin\eta=e^{\hat{\xi}}\sin\hat{\eta}-d \tag{5b}$$

holds.

The potential flow can be written as follows.

$$\psi=\psi_{\infty}(\xi,\eta)+\psi_0(\xi,\eta)+\psi_1(\hat{\xi},\hat{\eta}), \tag{6}$$

$$\psi_{\infty}=\cos\phi e^{\xi}\sin\eta-\sin\phi e^{\xi}\cos\eta, \tag{7a}$$

$$\psi_0=\sum_{k=0}^{\infty}(C_{0k}e^{-k\xi}\sin k\eta+D_{0k}e^{-k\xi}\cos k\eta), \tag{7b}$$

$$\psi_1=\sum_{k=0}^{\infty}(C_{1k}e^{-k\hat{\xi}}\sin k\hat{\eta}+D_{1k}e^{-k\hat{\xi}}\cos k\hat{\eta}), \tag{7c}$$

where ψ_{∞} represents the flow at infinity, and C_{0k}, D_{0k}, C_{1k} and D_{1k} are constants to be determined. The constants are determined so as ψ satisfies the impermeable condition at the surfaces. The method of successive improvement is used. That is, when C_{0k} and D_{0k} are to be obtained, C_{1k} and D_{1k} are given and vice versa. We illustrate the process of obtaining C_{0k} and D_{0k}. First, to impose the impermeable condition at the upper surface we must obtain $\psi_{10}(\eta)$, which is $\psi_1(\hat{\xi},\hat{\eta})$ evaluated at the upper surface. This is established by substituting into (7c) $\hat{\xi}=\hat{\xi}_0$ and $\hat{\eta}=\hat{\eta}_0$ obtained by (5a) and (5b) as follows.

$$\hat{\xi}_0=[\hat{\xi}]_{\xi=0}=\frac{1}{2}\ln(1+d^2+2d\sin\eta), \tag{8a}$$

$$\hat{\eta}_0=[\hat{\eta}]_{\xi=0}=\cos^{-1}(e^{-\hat{\xi}_0}\cos\eta). \tag{8b}$$

With α_{1k} and β_{1k} as the Fourier constants, $\psi_{10}(\eta)$ can be written as

$$\psi_{10}(\eta)=\sum_{k=0}^{\infty}(\alpha_{1k}\sin k\eta+\beta_{1k}\cos k\eta). \tag{9}$$

Then, the impermeable condition at the upper surface requires

$$D_{00}=-\beta_{10},$$
$$C_{01}=-\cos\phi-\alpha_{11},\quad D_{01}=\sin\phi-\beta_{11},$$
$$C_{0k}=-\alpha_{1k},\quad D_{0k}=-\beta_{1k}\ (k\geq 2).$$

Similar process applies in obtaining C_{1k} and D_{1k}. This process is repeated until converged values are obtained. The iteration scheme is conjectured to be stable since all the modes (except those of $k=0$) in ψ_0 and ψ_1 decrease exponentially with distance from the bodies.

The value of ψ at the upper surface is set zero, and that at the lower, ψ_{1w} is given by

$$\psi_{1w}=-d\cos\phi+\beta_{00}, \tag{10}$$

where β_{00} is the Fourier constant of the constant term of $\psi_{01}(\hat{\eta})$, which is $\psi_0(\xi,\eta)$ evaluated at the lower surface. The potential velocity u_p at the upper surface, u_{p0}, is obtained by the following formula.

$$\begin{aligned}u_{p0}(\eta)=&\left[-\frac{\partial\psi}{\partial\xi}\right]_{\xi=0}=-\cos\phi\sin\eta\\&+\sin\phi\cos\eta-\left[\frac{\partial\psi_0}{\partial\xi}\right]_{\xi=0}\\&+\frac{1}{h_1}\left[-\frac{\partial\psi_1}{\partial\hat{\xi}}\cos(\hat{\eta}-\eta)\right.\\&\left.+\frac{\partial\psi_1}{\partial\hat{\eta}}\sin(\hat{\eta}-\eta)\right]_{\xi=\xi_0,\eta=\eta_0},\end{aligned} \tag{11}$$

where $h_1=h_1(\eta)=e^{\hat{\xi}_0}$ is the size factor of the lower coordinate system at the upper surface. We can obtain $u_{p1}(\hat{\eta})$ for the lower surface from the similar formula.

The surface boundary conditions (3) for the Stokes problem are then

$$\Psi=0 \text{ at } \xi=0, \tag{12a}$$

$$\left[\frac{\partial\Psi}{\partial\xi}\right]_{\xi=0}=-\frac{3}{8}\left(\frac{du_{p0}^2}{d\eta}\right)$$

$$= \sum_{k=1}^{\infty} (E_{0k}\sin k\eta + F_{0k}\cos k\eta), \tag{12b}$$

for the upper cylinder, and

$$\Psi = \text{const. at } \xi = \xi_1, \tag{13a}$$

$$\left[\frac{\partial \Psi}{\partial \xi}\right]_{\xi=\xi_1} = -\frac{3}{8}\left(\frac{du_{p1}^2}{d\bar{\eta}}\right)$$

$$= \sum_{k=1}^{\infty} (E_{1k}\sin k\bar{\eta} + F_{1k}\cos k\bar{\eta}), \tag{13b}$$

for the lower cylinder, where $\xi_1 = \ln(\rho)$ is value of ξ at the lower surface, and the constants E_{0k}, F_{0k}, E_{1k} and F_{1k} are also obtained by the Fourier transform. It should be noted here that the series start from the mode $k=1$.

The series are truncated after $k=K$. To obtain the Fourier constants, the interval $0 \le \eta \le 2\pi$ is divided into J segments, each having the length $\Delta\eta = 2\pi/J$, and then the integration is performed by using the simplest scheme,

$$\int_0^{2\pi} g(\eta)d\eta = \sum_{j=1}^{J-1} g_j \Delta\eta,$$

for any integrand function $g(\eta)$.

4. Solution of the Streaming Flow

Choosing a suitable coordinate system is crucial in the whole solution techniques. The bipolar coordinate system is apparently convenient in imposing the surface conditions and the subsequent solution process. In the beginning of this study, therefore, the method of Zapryanov, Kozhoukharova and Iordanova (1988) based on the bipolar coordinates has been applied. However, it turned out that except for the special cases, that are treated by them, the far field flow velocity grows like $O(|z|)$. Such an unrealistic solution is attributed to the improper choice of the coordinate system or the impoper transform of Ψ (i.e. the equation shown at the lowest line of page 210 of the paper).

In this work, methods that give plausible solutions are developed using two separate coordinate systems as defined in §3. In the transformed planes, the governing Eg. (2) reads

$$\nabla_0^2 e^{-2\xi}\nabla_0^2\Psi = 0,\ \nabla_1^2 e^{-2\bar{\xi}}\nabla_1^2\Psi = 0, \tag{14}$$

for the upper and lower systems, respectively, where ∇_0^2 and ∇_1^2 are Laplacian operators for each system. We seek the solution in the form

$$\Psi = \Psi_c + \Psi_0(\xi,\eta) + \Psi_1(\xi,\bar{\eta}), \tag{15}$$

where Ψ_c is a constant.

Each of Ψ_0 and Ψ_1 is considered to be the sum of $f_{0k}(\xi)e^{ik\eta}$ and $f_{1k}(\xi)e^{ik\bar{\eta}}$, respectively, over $k \ge 0$, where $f_{0k}(\xi)$ (and similarly $f_{1k}(\xi)$) is a linear combination of four basis functions which are

$$\{1, \xi, e^{2\xi}, \xi e^{2\xi}\} \text{ for } k=0,$$
$$\{e^{-\xi}, e^{\xi}, \xi e^{\xi}, e^{3\xi}\} \text{ for } k=1,$$
$$\{e^{-k\xi}, e^{(2-k)\xi}, e^{k\xi}, e^{(k+2)\xi}\} \text{ for } k \ge 2.$$

If the model were composed of a single cylinder with the velocity specified at the surface, then it is abrupt to select the first two basis functions for every k. In this case, the far field flow velocity is at most $O(1)$ which is satisfactory. For the multiple cylinders, the same rule applies except for $k=1$.

The reason lies in the unique feature of the terms with the bases e^{ξ} and $e^{\bar{\xi}}$ for $k=1$. Consider, for instance, the modes $\Psi_0 = P_0 e^{\xi}\cos\eta$ and $\Psi_1 = P_1 e^{\bar{\xi}}\cos\bar{\eta}$, where P_0 and P_1 are arbitrary constants supposed for the moment to be independently determinative. By the transformation (5a), the resultant total mode can be written as $\Psi = \Psi_0 + \Psi_1 = (P_0 + P_1)e^{\xi}\cos\eta$ in terms of the upper coordinates and $\Psi = (P_0 + P_1)e^{\bar{\xi}}\cos\bar{\eta}$ in terms of the lower coordinates. Thus the two constants turned out to function as one in a combined form. In the physical sense, this is due to the fact that the terms with the bases e^{ξ} and $e^{\bar{\xi}}$ generate a 'uniform' flow everywhere. Consequently, we are left with $\{e^{-\xi}, e^{\xi}, e^{-\bar{\xi}}\}$ as the bases for $k=1$. We need one more basis function, which must be in a combined form $\xi e^{\xi} - \bar{\xi}e^{\bar{\xi}}$ so as to minimize the far field flow velocity; each separately generates $O(\ln|z|)$ velocity at infinity, but after combined $O(1/|z|)$.

Based on the above reasoning, we write Ψ_0 and Ψ_1 as follows.

$$\Psi_0(\xi,\eta) = Q_{00}\xi + (T_c\xi e^{\xi} + P_c e^{\xi} + Q_{01}e^{-\xi})\sin\eta + (U_c\xi e^{\xi} + R_c e^{\xi} + S_{01}e^{-\xi})\cos\eta$$

$$+\sum_{k=2}^{\infty}\Big[\ (P_{0k}e^{(2-k)\hat{\xi}}+Q_{0k}e^{-k\hat{\xi}})\sin k\eta+\ (R_{0k}e^{(2-k)\hat{\xi}}+S_{0k}e^{-k\hat{\xi}})\cos k\eta\Big], \tag{16a}$$

$$\Psi_1\ (\hat{\xi},\hat{\eta})=Q_{10}\hat{\xi}\ +\ (-T_c\hat{\xi}e^{\hat{\xi}}+Q_{11}e^{-\hat{\xi}})\sin\hat{\eta}+\ (-U_c\hat{\xi}e^{\hat{\xi}}+S_{11}e^{-\hat{\xi}})\cos\hat{\eta}$$
$$+\sum_{k=2}^{\infty}\Big[\ (P_{1k}e^{(2-k)\hat{\xi}}+Q_{1k}e^{-k\hat{\xi}})\sin k\hat{\eta}+\ (R_{1k}e^{(2-k)\hat{\xi}}+S_{1k}e^{-k\hat{\xi}})\cos k\hat{\eta}\ \Big], \tag{16b}$$

where all the Roman capital letters denote the unknown cosntants. The method of successive improvement is applied to obtain the constants. The method is basically similar to to that used in §3 except for $k=1$; the constants for $k=1$ are obtained in a partly implicit manner at each iteration step as will be described below.

First, we need to formulate $\Psi_{10}\ (\eta)$, which is $\Psi_1\ (\hat{\xi},\hat{\eta})$ evaluated at the upper surface. Suppose that $\hat{\xi}_0e^{\hat{\xi}_0}\sin\hat{\eta}_0$ and $\hat{\xi}_0e^{\hat{\xi}_0}\cos\hat{\eta}_0$ in (16b) are decomposed as

$$\hat{\xi}_0e^{\hat{\xi}_0}\sin\hat{\eta}_0=\tau_{1s}\sin\eta+\tau_{1c}\cos\eta$$
$$+\text{all the other modes},$$
$$\hat{\xi}_0e^{\hat{\xi}_0}\cos\hat{\eta}_0=\mu_{1s}\sin\eta+\mu_{1c}\cos\eta$$
$$+\text{all the other modes},$$

where τ_{1s}, τ_{1c}, μ_{1s} and μ_{1c} are constants. These terms are to be multiplied by $-T_c$ (in the first equation) and $-U_c$ (in the second). But we consider the constants for $\sin\eta$ and $\cos\eta$ as unknown and all the others as given; this is a key element for the numerical stability. (Similarly, in formulation of $\Psi_{01}\ (\hat{\eta})$, T_c and U_c multiplying the modes of $\sin\hat{\eta}$ and $\cos\hat{\eta}$ are considered as unknown.) Then we can write

$$\Psi_{10}\ (\eta)=-T_c\ (\tau_{1s}\sin\eta+\tau_{1c}\cos\eta)$$
$$-U_c\ (\mu_{1s}\sin\eta+\mu_{1c}\cos\eta)$$
$$+\sum_{k=0}^{\infty}\Big[\alpha_{1k}\sin k\eta+\beta_{1k}\cos k\eta\Big], \tag{17}$$

where the Fourier constants α_{1k} and β_{1k} differ from those used in §3. The impermeable condition (12a) then requires

$$\Psi_c=-\beta_{10}, \tag{18a}$$
$$-\tau_{1s}T_c-\mu_{1s}U_c+P_c+Q_{01}=-\alpha_{11}, \tag{18b}$$
$$-\tau_{1c}T_c-\mu_{1c}U_c+R_c+S_{01}=-\beta_{11}, \tag{18c}$$
$$P_{0k}+Q_{0k}=-\alpha_{1k}\ (k\geq 2), \tag{18d}$$
$$R_{0k}+S_{0k}=-\beta_{1k}\ (k\geq 2). \tag{18e}$$

To impose the velocity condition at the upper surface, we first need to formulate V_{10}, the tangential component of the velocity at the upper surface generated by Ψ_1. It can be shown that

$$V_{10}=\frac{1}{h_1}\Big[-\frac{\partial\Psi_1}{\partial\hat{\xi}}\cos\ (\hat{\eta}-\eta)$$
$$+\frac{\partial\Psi_1}{\partial\hat{\eta}}\sin\ (\hat{\eta}-\eta)\Big]_{\hat{\xi}=\hat{\xi}_0,\,\hat{\eta}=\hat{\eta}_0}$$

The same idea as that used in Eg. (17) is applied to write this as

$$V_{10}=T_c\ (\tau'_{1s}\sin\eta+\tau'_{1c}\cos\eta)$$
$$+U_c\ (\mu'_{1s}\sin\eta+\mu'_{1c}\cos\eta)$$
$$+\sum_{k=0}^{\infty}\Big[\gamma_{1k}\sin k\eta+\delta_{1k}\cos k\eta\Big],$$

where τ'_{1s}, τ'_{1c}, μ'_{1s}, μ'_{1c}, γ_{1k} and δ_{1k} are constants. Then the condition (12b) requires

$$Q_{00}=\delta_{10}, \tag{19a}$$
$$(1-\tau'_{1s})\,T_c-\mu'_{1s}U_c+P_c-Q_{01}$$
$$=\gamma_{11}-E_{01}, \tag{19b}$$
$$-\tau'_{1c}T_c+\ (1-\mu'_{1c})\,U_c+R_c-S_{01}$$
$$=\delta_{11}-F_{01}, \tag{19c}$$
$$(2-k)P_{0k}-kQ_{0k}$$
$$=\gamma_{1k}-E_{0k}\ (k\geq 2), \tag{19d}$$
$$(2-k)R_{0k}-kS_{0k}$$
$$=\delta_{1k}-F_{0k}\ (k\geq 2). \tag{19e}$$

We can obtain, for $k\geq 2$, P_{0k} and Q_{0k} from Eqs. (18d) and (19d), and R_{0k} and S_{0k} from Eqs. (18e) and (19e). A similar procedure applies in obtaining P_{1k}, Q_{1k}, R_{1k} and S_{1k} for $k\geq 2$, and the formula for these will not be presented.

The constants T_c, U_c, P_c, R_c, Q_{01} and S_{01} should be obtained with further conditions at the lower surface. A similar procedure is followed to obtain

$$\Psi_{1w}=Q_{10}\hat{\xi}+\beta_{00}+\Psi_c-P_cd, \tag{20a}$$
$$(-\rho\hat{\xi}_1+\tau_{0s})\,T_c+\mu_{0s}U_c+\rho P_c+\frac{1}{\rho}Q_{11}$$
$$=-\alpha_{01}, \tag{20b}$$
$$\tau_{0c}T_c+\ (-\rho\hat{\xi}_1+\mu_{0c})\,U_c+\rho R_c+\frac{1}{\rho}S_{11}$$
$$=-\beta_{01}, \tag{20c}$$

by imposing the condition (14a), and

$$Q_{10}=h_1\delta_{00}, \tag{21a}$$

$$(1+\xi_1+\tau'_{0s})T_c+\mu'_{0s}U_c-P_c+\frac{1}{\rho^2}Q_{11}$$
$$=-\gamma_{01}+E_{11}, \tag{21b}$$
$$\tau'_{0c}T_c+(1+\xi_1+\mu'_{0c})U_c-R_c+\frac{1}{\rho^2}S_{11}$$
$$=-\delta_{01}+F_{11}, \tag{21c}$$

by imposing (14b). Ψ_{1w} in Eq. (20a) denotes the value of Ψ at the lower surface. Now eight linear Eqs. (18b), (18c), (19b), (19c), (20b), (20c), (21b) and (21c) are solved to obtain eight unknowns T_c, U_c, P_c, R_c, Q_{01}, S_{01}, Q_{11} and S_{11}.

The iteration procedure is summarized as follows.

(i) Set all the constants in Eqs. (16a) and (16b) zero.

(ii) Compute the Fourier constants α_{0k}, $\cdots$, δ_{0k}, α_{1k}, $\cdots$, δ_{1k}.

(iii) Obtain Q_{00} by Eq. (19a) and Q_{10} by Eq. (21a).

(iv) Solve Eqs. (18d) and (19d) for P_{0k} and Q_{0k}, and Eqs. (18e) and (19e) for R_{0k} and S_{0k}, and similarly solve for P_{1k}, Q_{1k}, R_{1k} and S_{1k} (≥ 2).

(v) Solve 8 linear equations for T_c, U_c, $\cdots$,S_{11} as described above.

(vi) Repeat (ii) to (v) until all the values converge.

The truncation of the series and the integration scheme used in (ii) are as described in the last part of §3.

5. The Numerical Results

The effect of the series truncation, that is K, and the effect of the number of segments in the integration, that is J, are first studied. By a physical intuition, we expect that as the cylinders become closer K should be larger due to the stronger interaction between the cylinders. It was found that $K=40$ for $d=2.3$, 30 for 2.5, 20 for 3.0, 15 for 5.0 and 10 for 10.0 give the sufficiently accurate results. For most cases, $J=200$ is also found to be sufficient. The convergence becomes slower as d decreases by the same reason. For all cases presented in this paper, the number of iterations needed is less than 100. The computation time is negligibly small.

The potential flow solution obtained in this study is found to be very close to that given in terms of the bipolar coordinates (Morse and Feshbach 1953), which verifies the validity of the present numerical schemes.

Figure 2 shows streaming flow patterns for $\rho=1$ (equal cylinders), $d=5$, and three values of ϕ. The pattern of $\phi=0°$ is much similar to that of $\phi=90°$ except that the flow direction is opposite to each other, and more importantly that the former is a little stronger than the latter; such difference in the flow strength may be explained from the potential-flow configurations. We further note that the streaming flow is the strongest at $\phi=45°$. This can be explained by the fact that, while at $\phi=0°$ or 90° the streaming flow driven by the upper cylinder is interfered by that driven by the lower, at $\phi=45°$ each streaming flow is rather augmented. The interference effect may be associated with the number of cells N_c; we see that

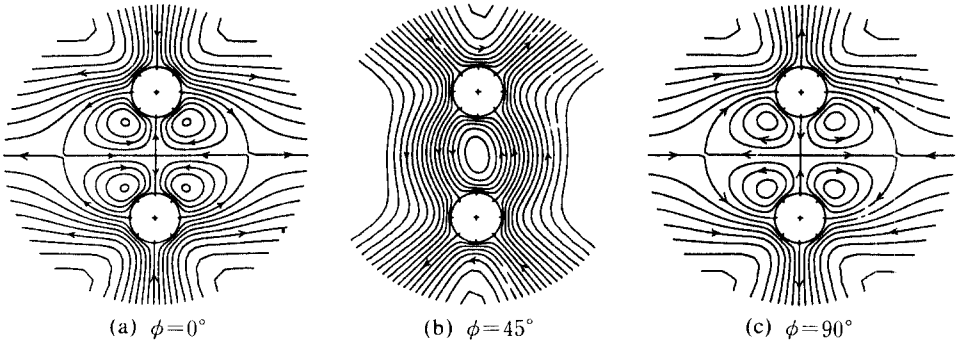

(a) $\phi=0°$ (b) $\phi=45°$ (c) $\phi=90°$

Fig. 2 Streaming flow patterns for $\rho=1$, $d=5$, and three values of ϕ. The increment of the stream function is 0.1.

$N_c=4$ for $\phi=0°$ and 90° and $N_c=1$ for $\phi=45°$. We note a slight asymmetry pattern for $\phi=45°$ which originates of course from the potential flow solution at small d; it is expected that the pattern becomes more symmetrical at larger d.

We may now extend these results to the cascade of circular cylinders, where infinite cylinders are arranged in a line (Fig. 3). For $\phi=0°$ or 90°, it is conjectured that the four-cell pattern similar to Fig. 2 (a) or (c) is repeated resulting in a very weak flow in the far field (Fig. 3 (a)); the case of $\phi=0°$ has been studied by Yan et al. (1993). For $\phi=45°$, it is also conjectured that the single-cell pattern similar to Fig. 2 (b) is repeated resulting in an almost uniform downward flow in the left far-field and an almost uniform upward flow in the right far-field (Fig. 3 (b)). It is interesting to note that such a far-field flow configuration is qualititively similar to that observed by Yan et al. (1993) for $\phi=0°$ at $R_s>9$.

We next investigate the bifurcation of flow patterns with ϕ as the bifurcation parameter. Here, a bifurcation sets in when the flow pattern is qualititively changed with ϕ. Figure 4 shows eight flow patterns given by six bifurcations (Fig. 4 (b) and (c) are of the same pattern) in the interval $0°\leq\phi\leq90°$. Identification of flow patterns like Fig. 4 is important e.g. in migration of particles as stated in §1.

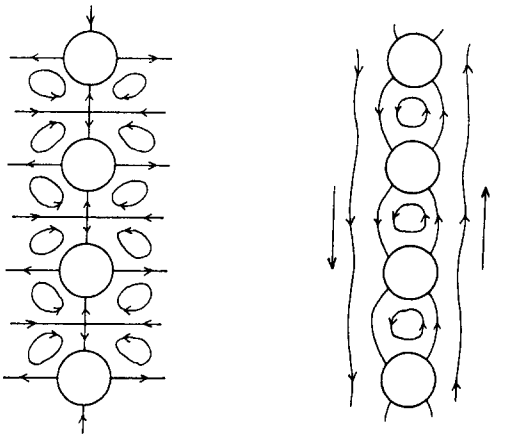

(a) $\phi=0°$ (b) $\phi=45°$

Fig. 3 Sketch of the conjectured flow patterns for $\phi=0°$ and 45° around the cascade of circular cylinders arranged in a line.

The flow pattern becomes more complicated in the gap region as the cylinders come closer. Figure 5 shows such variation for $\rho=1$, $\phi=60°$ and three values of d. We first note that there are two small cells for $d=2.8$ (Fig. 5 (a)) which do

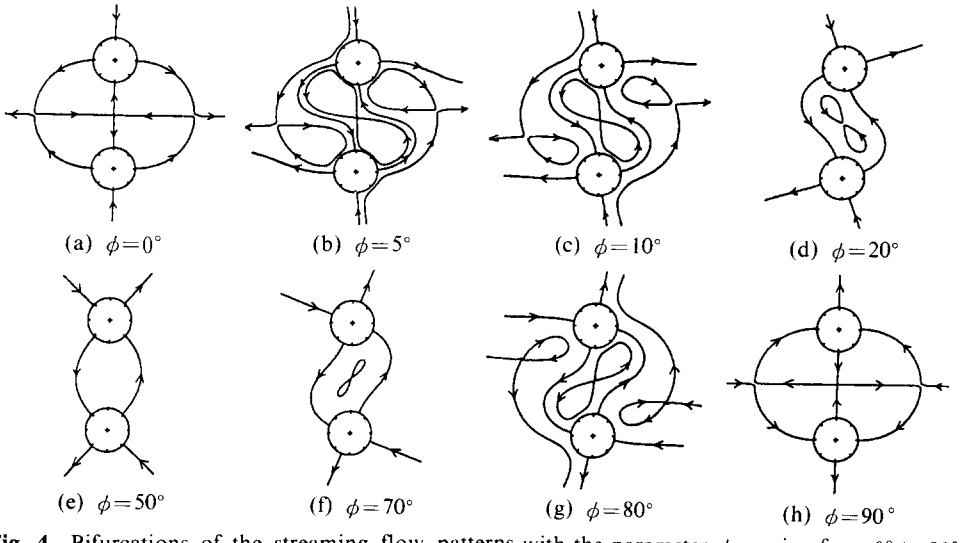

(a) $\phi=0°$ (b) $\phi=5°$ (c) $\phi=10°$ (d) $\phi=20°$

(e) $\phi=50°$ (f) $\phi=70°$ (g) $\phi=80°$ (h) $\phi=90°$

Fig. 4 Bifurcations of the streaming flow patterns with the parameter ϕ varying from 0° to 90°. The patterns (b) and (c) are representative of the paramatric domain $0°<\phi<16.5°$. The pattern (d) is for $16.5°<\phi<29.0°$, (e) for $29.6°<\phi 66.8°$, (f) for $66.8°<\phi 75.7°$, (g) for $75.7°<\phi<90°$.

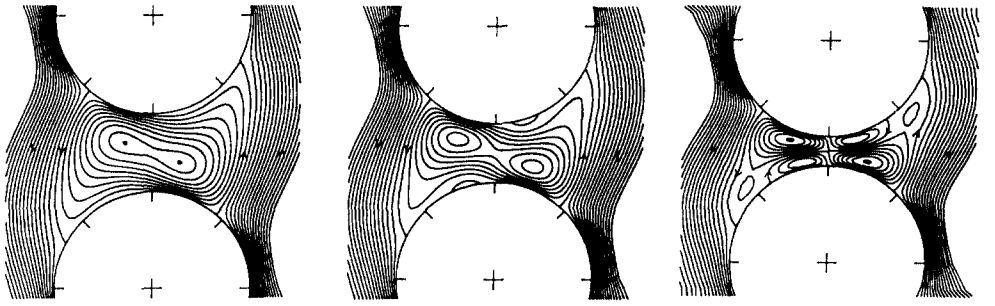

(a) $d=2.8$ (b) $d=2.6$ (c) $d=2.3$

Fig. 5 Streaming flow patterns in the gap region for $\phi=600$, and three small values of d. The increment of the stream function is 0.02 except for $\Psi=0.17$ repre senting two small cells in (a).

not exist at $d=5.0$ (Fig. 4 (e)). These are more pronounced as d decreases (Fig. 5 (b)). This phenomenon is due to two facts. First, distribution of the surface streaming velocity u_s is more localized as d decreases; for instance u_s in the left-hand side becomes larger while that in the right-hand side becomes smaller for the upper cylinder. Second, decrease of d does not move the two separating streamlines significantly, causing the confined region more pinched in the middle. We next note that two additional small cells appear at $d=2.6$ (Fig. 5 (b)) near the surface of the cylinders. These cells become larger and stronger at $d=2.3$ (Fig. 5 (c)). Appearance of those cells are attributed to a peculiar pattern in the potential flow at small d values. Figure 6 shows a typical streamline pattern of the potential flow. We note that the passage between two separating streamlines (including the body lines) undergoes two more diverging-converging effects than the one at moderate or large values of d. Addition of two diverging-converging places yields four additional stagnation points in the streaming flow field at the cylinder surfaces, which in turn gives rise to two additional cells. Growth of the two cells then results in generation of two weak cells (Fig. 5 (c)).

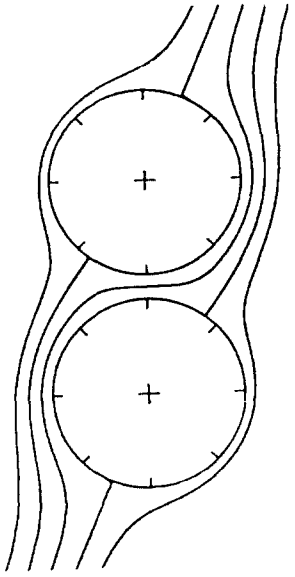

Fig. 6 A typical streamline pattern of the potential flow when two cylinders are very close; $d=2.255$, $\phi=70°$. The increment of the stream function is 0.0891.

We should note here two things for the case of small d (such as Fig. 5 (c)). Firstly, for the classical asymptotic-expansion-method to be valid, the ratio of the oscillation amplitude (U_0/ω) and the gap spacing (2a-d), or U_0/ω (2a-d), must be small enough. This is severer than the restriction $\varepsilon\ll 1$ as specified in the first paragraph of §2. Secondly, we need more terms (larger K) in the series for small d, and it is consistent with the fact that, also in the discretizing method, the convergence becomes slower at smaller d as pointed out by one of the refrees from his experience in the related numerical computation.

6. Conclusions

A series solution method is developed in this

study for two-dimensional low-Reynolds-number flows around two circular cylinders of different radii with arbitrary arrangement relative to the direction of the oscillatory motion of the fluid. It is abrupt to extend this idea to a group of cylinders more than two.

Calculations for two equal cylinders show that the streaming flow for $\phi=45°$ is much stronger than that for $\phi=0°$ or 90°. Bifurcation in the flow pattern is studied with ϕ as the parameter. At $d=5$, six bifurcations take place. As two cylinders come closer, the flow pattern in the gap region becomes more complicated due to basically to emergence of two additional diverging-converging flows between the separating streamlines in the potential flow field.

In the future, solutions for two cylinders with different radii will be presented, and the case of three and four cylinders will also be studied.

Acknowledgement

This work is supported by Korea Ministry of Education through Mechanical Engineering Research Fund (ME94-C-02).

References

Batchelor, G. K., 1977, *An Introduction to Fluid Dynamics. Cambridge University Press.*

Davidson, B. J., 1973, "Heat Transfer from a Vibrating Circular Cylinder," *Int. J. Heat Mass Transfer*, Vol. 16, p. 1703.

Haddon, E. W. and Riley, N., 1981, "The Heat Transfer Between Concentric Vibrating Circular Cylinders," *Q. J. Mech. Appl. Maths*, Vol. 34, p. 345.

Jeffery, G. B., 1922, *Proc. R. Soc. London A*, Vol. 101, p. 169.

Kim, S. K. and Troesch, A. W., 1989, "Streaming Flows Generated by High-Frequency Small-Amplitude Oscillations of Arbitrarily Shaped Cylinders," *Phys. Fluids A*, Vol. 1, pp. 975~985.

Krasuk, J. H. and Smith, J. M., 1963, "Mass transfer in a pulsed column," *Chem. Engrg Sci.*, Vol. 18, p. 591.

Morse, P. M. and Feshbach, H., 1953, *Methods of Theoretical Physics*. McGraw-Hill Book Co.

Pattani, P. G. and Olson, M. D., 1987, "Periodic Solutions of Rigid Body-Viscous Flow Interaction," *Int. J. Num. Meth. Fluids*, Vol. 7, pp. 653~695.

Riley, N., 1967, "Oscillating Viscous Flows, Review and Extension," *J. Inst. Math. Applics*, Vol. 3, pp. 419~434.

Smith, S. H., 1990, "Some Limitation of Two-Dimensional Unbounded Stokes Flow," *Phys. Fluids A*, Vol. 2, pp. 1724~1730.

Stuart, J. T., 1966, "Double Boundary Layers in Oscillating Viscous Flows," *J. Fluid Mech.*, Vol. 24, pp. 673~687.

Yan, B., Ingham, D. B. and Morton, D. B., 1993, "Streaming Flow Induced by an Oscillating Cascade of Circular Cylinders," *J. Fluid Mech.*, Vol. 252, pp. 147~171.

Zapryanov. Z., Kozhoukharova, Zh and Iordanova, A., 1988, "On the Hydrodynamic Interaction of Two Circular Cylinders Oscillating in a Viscous Fluid," *J. Appl. Math. Phys.*, Vol. 39, pp. 204~220.